2015

Energy Dissipation and Constitutive Modeling for a Mechanistic Description of Pad Scratching in Chemical-Mechanical Planarization

David Ponte
University of Rhode Island

D.M.L. Meyer
University of Rhode Island, dmmeyer@uri.edu

Citation/Publisher Attribution
Ponte, D.C. & Meyer, D.M.L. J Mater Sci: Mater Electron (2016) 27: 1745. doi: 10.1007/s10854-015-3949-4
Available: http://dx.doi.org/10.1007/s10854-015-3949-4

Energy Dissipation and Constitutive Modeling for a Mechanistic Description of Pad Scratching in Chemical-Mechanical Planarization

David C. Ponte[1] and D. M. L. Meyer[1,*]

[1] Mechanical Engineering, University of Rhode Island, Kingston, RI, USA

* Corresponding author:

Email: dmmeyer@uri.edu

Tel: (401) 874-9292

Fax: (401) 874-2355

Journal of Materials Science: Materials in Electronics

1 Introduction

Chemical-mechanical planarization (CMP) is a necessary step in the fabrication of state-of-the-art integrated circuits (ICs). With a process that requires accuracy and precision to the nanoscale, CMP is a challenging process to achieve high manufacturing yields. It has only recently been reported in the literature that IC wafer defects can be produced from the polishing pad material itself [1]. Relatively soft polishing pads can induce scratches on harder wafers that are large enough to greatly reduce manufacturing yields. Previous work investigating CMP pad scratching provides mechanical criteria based on contact mechanics which can predict scratching and presents methods to reduce damage [1-3]. Pad scratches are mitigated by decreasing relative hardness values of the pad and wafer materials, decreasing the coefficient of friction between the pad and wafer, and flattening the pad topography. Experimental results from this work indicated that not all pad scratches are eliminated from CMP with one or more of these criteria.

Past work is expanded upon in the current research by formulation of a comprehensive mechanistic model for the process of pad scratching. Thermomechanical processes that occur during CMP and pad scratching are investigated though various approaches. Experimental replication of the CMP process is performed to obtain tribological information of IC1000 pad material and wafer contact through CMP. Pad material is sampled throughout the planarization experiments for additional constitutive characterization. The mechanical behavior of the IC1000 pad is experimentally measured to model the material's viscoelastic behavior and quantify its compressibility. Differential scanning calorimetry (DSC) of new and used pad samples is conducted to investigate energy dissipation into the pad material surface. The resulting thermomechanical information for CMP provides a more complete physical understanding of pad scratching as well as the general CMP process.

2 Methodology

To understand the mechanisms of scratching by the softer pad on the harder wafer material, mechanical and thermal processes that occur during CMP are analyzed. A thermomechanical model of the scratching process is formulated to account for the input energy that is dissipated through the pad scratching process. Scratching is represented as a plastic deformation of the wafer surface, the dissipation of energy, and an increase in entropy. To account for damage produced by pad scratching, laws of thermodynamics are applied. All energy that is input into the system from the applied pad tractions is accounted for using the first law of thermodynamics, also known as conservation of energy. This law states that all energy of a system cannot be destroyed and must be conserved, all due to the interconvertibility of the energetic processes. In the case of chemical-mechanical planarization, the system of interest includes the polishing pad, wafer, and slurry. The relation for the conservation of the time rate of change of energy at any point in a continuum is Equation 1 [4],

$$\rho \frac{\mathrm{D}u}{\mathrm{D}t} = \boldsymbol{\sigma} : \boldsymbol{D} - \operatorname{div} \bar{q} + \rho r \tag{1}$$

ρ is the mass density, u is the internal energy per unit mass, $\boldsymbol{\sigma}$ is the Cauchy stress tensor, $\boldsymbol{D}$ is the rate of deformation tensor, $\bar{q}$ is the heat flux vector, and r is the heat supply per unit mass. The Cauchy stress tensor is assumed to be symmetric in this description.

From the first law of thermodynamics, the energy input to the pad and wafer contact must be conserved. In CMP, all of the energy that is input to the wafer is from the pad's applied tractions. Part of this energy is dissipated through processes that include damaging the wafer material through scratching. To account for the energy dissipation, the second law of thermodynamics in the form of the Clausius-Duhem inequality is applied for any point in a continuum, given in Equation 2 [4],

$$\frac{\mathrm{D}\eta}{\mathrm{D}t} \geq -\mathrm{div}\left(\frac{\bar{q}}{\Theta}\right) + \frac{\rho r}{\Theta} \tag{2}$$

η is the entropy per unit mass and Θ is the absolute temperature. Entropy that fluxes into the system may be in the form of sensible heat, mass, and acoustics, among other forms, as represented by -div $\left(\frac{\bar{q}}{\Theta}\right)$. The entropy that is formed within the system is represented as configurational entropy, and is symbolized as $\frac{\rho r}{\Theta}$. Part of the configurational entropy changes of the material result from plastic deformation among other potential dissipation processes. The main goal is the decomposition of the individual processes contributing to the configurational entropy changes of the CMP process to determine exactly how the wafer is being deformed from the applied tractions of the polishing pad. Also, additional dissipation processes that may have an influence on scratch production can be accounted for.

More explicit descriptions of energy dissipation processes are obtained by combining Equation 1 and 2 to result in Equation 3,

$$\rho\Theta\dot{\eta} \geq \rho\dot{u} + \frac{1}{\Theta}(\bar{q} \cdot \overline{\nabla}\Theta) - \boldsymbol{\sigma} : \boldsymbol{D} \tag{3}$$

The dot accent represents the material derivative with respect to time. When applied to chemical-mechanical planarization, all of the terms in Equation 3 provide the means to account for individual dissipation processes that occur in pad scratching. It is with this equation that no assumptions are made to remove potential sources of dissipation.

For the system of CMP, ρu̇ represents the rate of change of internal energy of the CMP materials. The flux term $\frac{1}{\Theta}(\bar{q} \cdot \overline{\nabla}\Theta)$ symbolizes the flux of energy dissipation. The term $\boldsymbol{\sigma} : \boldsymbol{D}$, that includes the Cauchy stress tensor and the rate of deformation tensor, represents the rate of strain energy in the pad and wafer materials. This term can be assembled into different forms of strain energy by decomposing the stress and rate of deformation terms. The Cauchy stress tensor and rate of deformation tensor can be described by their elastic and plastic components given in Equation 4 [5, 6],

$$\boldsymbol{\sigma} : \boldsymbol{D} = \boldsymbol{\sigma}^{\boldsymbol{e}} : \boldsymbol{D}^{\boldsymbol{e}} + \boldsymbol{\sigma}^{\boldsymbol{p}} : \boldsymbol{D}^{\boldsymbol{e}} + \boldsymbol{\sigma}^{\boldsymbol{e}} : \boldsymbol{D}^{\boldsymbol{p}} + \boldsymbol{\sigma}^{\boldsymbol{p}} : \boldsymbol{D}^{\boldsymbol{p}} \tag{4}$$

$\boldsymbol{\sigma}^{\boldsymbol{e}}:\boldsymbol{D}^{\boldsymbol{e}}$ represents elastic strain energy that is the time-independent strain energy associated with the pad and wafer; $\boldsymbol{\sigma}^{\boldsymbol{p}}:\boldsymbol{D}^{\boldsymbol{e}}$ represents viscoelastic strain energy that has time-dependent viscous effects; $\boldsymbol{\sigma}^{\boldsymbol{e}}:\boldsymbol{D}^{\boldsymbol{p}}$ represents elasto-plastic strain energy that has history-independent, yet time-dependent effects; $\boldsymbol{\sigma}^{\boldsymbol{p}}:\boldsymbol{D}^{\boldsymbol{p}}$ represents the fully plastic strain energy that has history-dependent and time-dependent effects. Determination of the relative importance that each form of energy dissipation

contributes to the total input energy dissipation provides important information about the mechanisms of pad scratching. In the current work, multiple forms of energy dissipation are investigated experimentally. The main focus is on the thermomechanical behavior of polyurethane foam polishing pad material, with its complex material behavior.

3 Experimental

3.1 Planarization Experiments

The CMP process was replicated to obtain direct experimental information about the planarization process. A reciprocating linear tribometer in Fig. 1, fabricated in-house, was used to conduct planarization experiments. For each test type, plates of either high purity copper or silicon dioxide wafer materials were fixed to the reciprocating positioning table. A layer of polishing slurry (Dow ACuPlane, Midland, MI) was held on the wafer surface with the slurry tray. A sample of IC1000 (Rohm and Haas Co., Philadelphia, PA) grooved polishing pad material was soaked for approximately 14 hours, adhered to the pad fixture and then loaded onto the wafer surface using the pneumatic cylinder. The positioning table reciprocated at one of two speeds for a number of cycles with the pad and wafer materials in contact. Multiple trials were completed to account for a wide range of velocities and pressures that occur in CMP. Experiments were performed at average velocities of 0.2 m/s or 0.6 m/s. Normal pressures applied were 14 kPa or 34 kPa. Eight total trials were conducted with all four combinations of velocity and pressure levels for copper and silicon dioxide wafer materials.

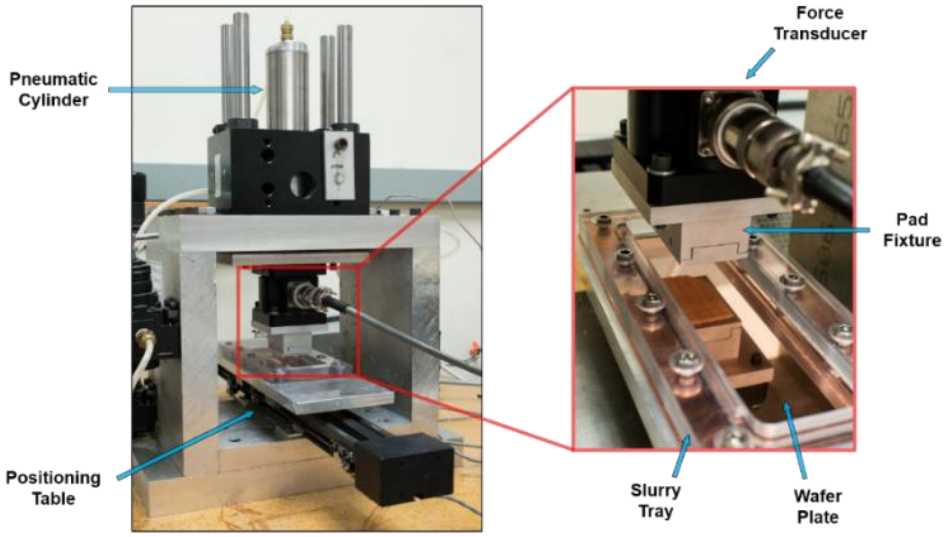

Fig. 1 Reciprocating Linear Tribometer

The contacting pad and copper or silicon dioxide substrates traveled a total sliding distance equivalent to the time required to polish 250 wafers. This polishing time is based on the maximum time that a point on the pad is in contact when polishing a wafer. The conditions used in this computation were for a pad diameter of 500 mm and a wafer diameter of 200 mm that is polished for 60 seconds, as these are common specifications for CMP processes [7, 8]. The total resulting time the pad samples traveled in contact with the substrates was approximately 90 minutes. The contact distance traveled for the low

velocity experiments was approximately 1,100 meters, and contact distance for the high velocity experiments was approximately 3,200 meters. Intermittently, the experiments were stopped to collect samples of pad material at an equivalent 10, 50, 100, and 250 wafers polished. A dynamometer (AMTI MC3A-6-250, Watertown, MA) was used to measured voltages which were then converted into contact forces that act between the pad and wafer surfaces.

3.2 Surface Profilometry

Measurements of the pad surface topography were conducted using a surface profilometer (Mahr Federal Perthometer, Göttingen, Germany) and MarSurf XR 20 software. A travel length of 5.6 mm and a travel velocity of 0.5 mm/s were used for all measurements. A short bandwidth filter of 2.5 μm and a cut off wavelength of 0.8 mm were used to compute average and root mean squared roughness of the pad surfaces.

3.3 IC1000 Pad Stress Relaxation

Stress relaxation experiments on the IC1000 pad material were performed to mechanically characterize the time dependent behavior of the material to determine its significance. Polishing pads are usually viscoelastically characterized in tension or bending, even though the pads are placed under compression during CMP [9-11]. Stress relaxation experiments in this work were performed in both compression and tension to additionally observe potential behavioral differences of the pad depending on the mode of loading.

3.3.1 Compression Stress Relaxation

Experiments for compression stress relaxation were performed using a fabricated material compression testing setup which is presented in Fig. 2. A sample of pad material was placed between the aluminum blocks and displacement was applied to the sample using a micrometer (Newport Research Corp. SM-50 Vernier, Irvine, CA). A 5 kg load cell (Phidgets CZL635, Calgary, Alberta, Canada) was used to continuously measure the load that was applied to the pad material. Displacement was applied at a near constant rate for approximately 5 seconds, and after that time the micrometer movement was halted. It was at this point that strain on the pad material was held constant and the peak load was applied to pad sample. The load relaxation of the sample was then measured for 4000 seconds after the peak load. This load was converted into a nominal stress based on the nominal area of the pad sample.

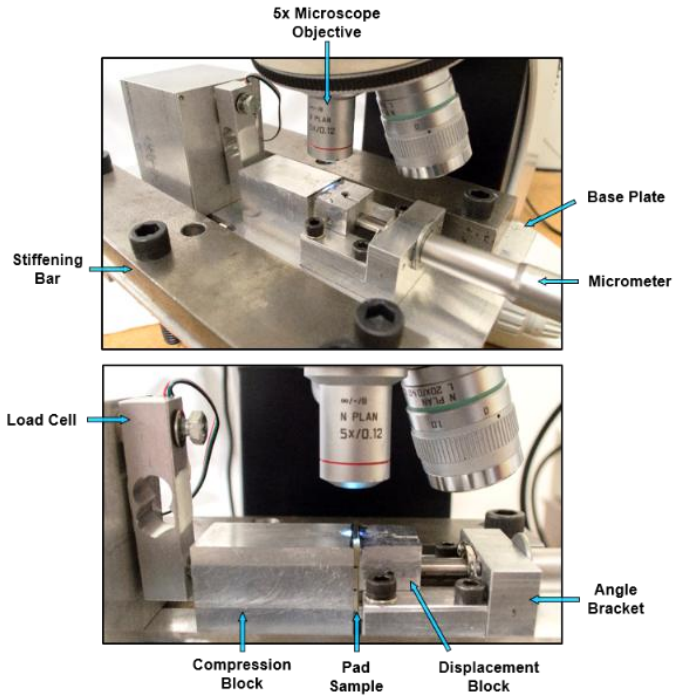

Fig. 2 Material Compression Testing Setup

Pad samples in different conditions were tested. These conditions included new and unused pad samples, new and soaked pad samples, and used pad samples after the equivalent of polishing 10, 50, 100 and 250 wafers. The soaked pad samples were soaked in slurry or separately in distilled water for at least 14 hours. Some samples were tested right after being soaked while still wet, while others were allowed to dry completely. The used pad samples were taken from the performed planarization experiments in this work. Some sample types were tested multiple times and the results averaged together in an attempt to remove variations between trials. These trials were performed to an initial stress of 4 psi or 27.6 kPa, as this is a common normal pressure applied in CMP [8, 12]. Additional trials were performed on new pad samples to view the effects of stress magnitude on the relaxation behavior of the pad material. Pad samples tested had compression face rectangular dimensions of approximately 13 mm by 19 mm.

3.3.2 Tensile Stress Relaxation

A high precision universal vertical load machine (Instron 3345, Canton, MA) was used to perform tensile stress relaxation experiments on pad samples with an approximate width of 25 mm and gauge length of 100 mm. The grooves of the samples were always oriented along the direction of loading to remove variations in mechanical behavior due to the influence of the grooves. For each trial, strain was applied at a linear rate for 0.6 seconds when the desired strain value is reached and subsequently held. Trials were run for constant strains of 0.25%, 0.50%, 1.0%, 1.5%, 2.5%, and 5.0%. The relaxation of load over 16 minutes was measured. Values of average stress were estimated using the sample width and average thickness of the grooved pad.

3.4 IC1000 Pad Compressibility

When modeling the true stresses of a compressible material, it is important to know the level of compressibility at the deformation state of interest. Since the IC1000 pad material is a porous foam, it is hypothesized to have a significant amount of compressibility. The relation for true stress is given in Equation 5 [4],

$$\boldsymbol{\sigma} = \frac{1}{J}\boldsymbol{P}\boldsymbol{F}^{\boldsymbol{T}} \tag{5}$$

J is the Jacobian, $\boldsymbol{P}$ is the Piola-Kirchhoff stress tensor, and $\boldsymbol{F}$ is the deformation gradient tensor. The Jacobian is a measure of compressibility of the material being modeled, represented mathematically in Equation 6,

$$J = |\mathrm{Det}\,\boldsymbol{F}| = \frac{\mathrm{d}V}{\mathrm{d}V_o} \tag{6}$$

The Jacobian is equal to the current volume divided by the un-deformed volume. Thus, the compressibility of the IC1000 pad material is required for proper computation of the true stress in the polishing pad.

Compressibility of the polishing pad was measured using the same fabricated compression testing setup shown in Fig. 2. Rectangular polishing pad samples with approximately 1.5 mm length sides were compressed between the blocks of the compression test setup. Using a microscope (Leica Microsystems Inc. DMLB, Bannockburn, IL) and CCD camera (Watec WAT-902A, Newburgh, NY), a grayscale video of the pad sample was captured as it was compressed. The video frames were imported into MATLAB (Mathworks, Inc., Natick, MA) to apply the Image Processing Toolbox to isolate the pad sample from the background with a binary filter. The width and thickness of the pad sample were computed from the binary images for each frame. Images of a pad sample from before compression and after full compression are seen in Fig. 3a, b. The respective binary sample isolated images are in Fig. 3c, d. Pad samples were compressed to a maximum of 20% strain for each of the eight trials performed.

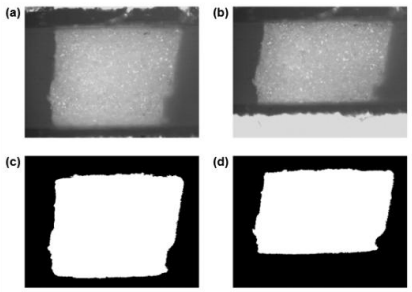

Fig. 3 Images of IC1000 Pad Sample Compression **(a)** 0% Strain in Grayscale, **(b)** 18% Strain in Grayscale, **(c)** 0% Strain in Binary, **(d)** 18% Strain in Binary

Assuming the pad sample face that is compressed is square, the volume of the sample for each frame was estimated by the computed thickness and width values. The value for the Jacobian, Poisson's ratio, and strain dilatation of the pad samples were estimated with these measurements.

3.5 IC1000 Pad Differential Scanning Calorimetry (DSC)

Energy that is dissipated into the internal structure of the IC1000 polishing pad during CMP was investigated using differential scanning calorimetry (DSC). Any significant internal energy dissipation could provide clues to identify how the pad surface has chemically and mechanically changed through CMP by calculating the enthalpies of reaction (*H*) from the integration of the heat flow into the pad samples over a temperature range. For these experiments, a TA Instruments Q10 DSC was used (TA Instruments, New Castle, DE). A single point temperature calibration using an indium sample was performed for proper instrument calibration. Six IC1000 unused pad samples were tested in the DSC to obtain base information about the polishing pad material. To observe changes to the polishing pad internal structure through polishing, thirty-two used pad samples from planarization experiments were tested in the DSC. The samples were prepared by shaving off the top layer of the pad surface so the material better represented that which was in contact with the wafer. Pad samples between 2 mg and 5 mg were placed into unsealed aluminum pans to maintain a constant pressure environment. The DSC cell was purged with 50 ml/min of nitrogen gas. Constant heating and cooling rates of 10°C/minute were used. The temperature program began at an initial temperature of 30°C, heated to 225°C for the first heat, cooled to -75°C, and heated to 225°C for the second heat.

The output data of the DSC is heat flow and temperature. To compute heat capacities and enthalpies of reaction for the pad samples, Equations 7 and 8 are utilized [13],

$$C_p = \left(\frac{\delta q}{\mathrm{d}t}\right)_p \frac{\mathrm{d}t}{\mathrm{d}\theta} \tag{7}$$

$$\Delta H = \int_{T_A}^{T_B} C_p \mathrm{d}\theta \tag{8}$$

C_p is the heat capacity, $\frac{\delta q}{\mathrm{d}t}$ is the heat flow, $\frac{\mathrm{d}\theta}{\mathrm{dt}}$ is the temperature rate, and *H* is the enthalpy. The heat capacity and enthalpies were normalized by mass of the sample to acquire specific heat and specific enthalpy.

4 Wafer Stress Field Analysis

A contact stress analysis between the pad and wafer was conducted to predict the mechanical conditions that allow for scratches to be produced on the wafer surface. In this analysis, scratching is assumed to occur when the wafer material reaches its mechanical yield stress. It is at this stress level that the wafer plastically deforms. To approximate the wafer stress field which produces scratches, the contact stresses associated with a single pad asperity are determined analytically. The average surface roughness of the IC1000 pad is two orders of magnitude larger than the wafer material surface roughness. The geometry of the contact is assumed to be a spherical pad asperity in contact with a flat wafer half-space, as is depicted in Fig. 4. The asperity is loaded onto the wafer while moving at velocity V in the negative x direction. The origin is at the center of the circular contact with a contact diameter 2*a*. The total tractions, *p*(*x*), produced on the wafer surface are due to normal pressure of the pad on the wafer, and friction from the sliding contact.

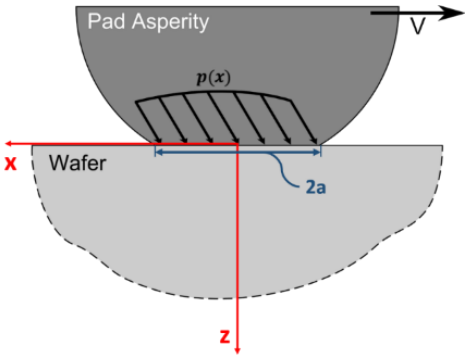

Fig. 4 Pad Asperity and Wafer Contact

The wafer is modeled as a linearly elastic material before yield. It has been shown that the polishing pad material plastically deforms and has time dependent mechanical behavior in CMP [3, 9-11]. The desired result of this analysis is to determine the elementary contact mechanics variables that influence scratch production. This analysis assumes the pad material to be linear elastic for small strains of the pad asperity. Additionally, all materials are assumed to be isotropic and homogeneous. The stress field of a circular sliding contact with friction has been solved by Goodman and Hamilton [14, 15]. Quasi-static stress fields in an elastic surface from tractions of a sliding spherical asperity were determined in closed form solutions. This solution is based on the superposition of a Hertzian normal pressure distribution and a tangential shear traction that is proportional to the normal pressure by the coefficient of friction. These tractions act within the contact circle of radius *a*.

The von Mises yield criterion is applied to the wafer material, which states that if the von Mises stress is greater than or equal to the yield stress of the material, then the material plastically deforms. Hamilton and Goodman state that the value of maximum von Mises stress moves to the surface of the linear elastic material when the coefficient of friction is larger than 0.3, which is expressed by Equation 9 [14, 15],

$$\sigma_v = \frac{3P}{2\pi a^2}\left[\frac{(1-2\nu)^2}{3} + \frac{(1-2\nu)(2-\nu)\mu\pi}{4} + \frac{(16-4\nu+7\nu^2)\mu^2\pi^2}{64}\right]^{1/2} \tag{9}$$

P is the total normal load, μ is the coefficient of friction, *a* is the contact radius, and ν is the Poisson's ratio of the wafer. Equation 9 provides the yield criterion for a relatively soft elastic sliding pad asperity over the harder wafer surface [3, 14, 15].

The scratching ability of the polishing pad increases with a greater load of the contact, greater coefficient of friction, and smaller contact area of the asperity. A polishing pad that will reduce pad scratching has a smaller elastic modulus, a smaller coefficient of friction against wafer materials, and a smoother surface. The real contact between a polishing pad and a wafer consists of many pad asperities in contact. A decrease in the deviation of asperity peaks on the pad surface will distribute the total load on the wafer more evenly, reducing the maximum total load for single asperity contacts [3]. Increasing the asperity radius of curvature increases the area of contact. Thus, a generally smoother pad surface reduces its ability to scratch the wafer.

Since the pad is a viscoelastic material, the stresses and strains of the CMP contact are time dependent. If a constant compressive displacement were applied to the sliding asperity, the normal load produced would decrease with time. This constant displacement boundary condition is similar to that of a stress relaxation experiment. The von Mises stress on the wafer from a single asperity would thus decrease over time as the load relaxes. With a constant load boundary condition, the pad asperity will creep and displace into the wafer. The contact radius will increase and disperse the load over a larger area. With the increase in time of contact, the ability for the pad asperity to scratch the wafer also increases. A polishing pad with viscoelastic behavior thus has an influence on scratch production.

5 Results and Discussion

5.1 Coefficient of Friction for Pad and Wafer Contact

From the performed planarization experiments, coefficients of friction between the pad and wafer contact had a general decreasing trend with increasing polishing time. The average coefficient of friction between the pad and wafer for all eight experiments performed for the first minute traveled was 0.32. For the last minute of travel before completion of the total 90 minutes of travel time, the average coefficient of friction between the pad and wafer was 0.21. Wafer material type showed that the substrate material had an effect on the force of friction with significant differences in coefficients of friction between pad on copper and pad on silicon dioxide. For the pad articulating against a copper substrate, the initial and final average coefficients of friction are 0.35 and 0.26, respectively. For the pad against a silicon dioxide substrate, the initial and final average coefficients of friction are 0.29 and 0.16, respectively. There is a general decreasing trend in coefficients of friction between the pad and wafer materials with increasing polishing time. The ability for the pad to scratch the wafer decreases with pad use, since the coefficient of friction decreases the stress on the wafer surface. These experiments additionally showed that the coefficients of friction between the pad and silicon dioxide are significantly less than for the contact between the pad and copper wafer substrates.

5.2 Pad and Wafer Topography

Average surface roughness along the length and across the width of the four copper surfaces planarized started at 0.060 μm. Since the sample on the linear tribometer travels in two directions along the same line of contact, wafer surface topography is measured parallel and perpendicular to the length of travel after planarization. After the total polish time equivalent to 250 wafers polished, average roughness along the length and across the width of copper wafer surfaces were an average of 0.026 μm and 0.061 μm, respectively. The four silicon dioxide surfaces began with an average surface roughness of 0.011 μm. After the total polish time equivalent to 250 wafers polished, average roughness along the length and across the width of silicon dioxide wafer surfaces were an average of 0.010 μm and 0.085 μm. These results indicate that there was a general smoothing of the surface across the length of travel, as expected with the pad material wearing the wafer in the same direction with each pass. An increase in the surface roughness perpendicular to the length of travel is a result of scratches formed during planarization.

A new pad surface was measured to have an average roughness of 3.97 µm and a root mean square roughness of 5.05 µm. Pad samples that were taken from each of the eight planarization experiments had a general decrease in the surface roughness with polishing time. The mean value of the average roughness of the pad samples at 250 wafers polished was 3.08 µm, while the mean value of the root mean square roughness for these samples was 4.12 µm.

From the smoothing of the pad surface asperities, it appears that the pad material surface is plastically deforming through planarization. These results suggest that plastic strain energy into the pad material has a significant influence on the scratch generation process. The pad surface becomes smoother and the coefficient of friction decreases with increasing polishing time, thus reducing the scratching ability of the polishing pad. Additional controlled experiments that isolate the pad surface roughness variable would have to be performed to confirm the potential correlation between pad surface roughness and coefficient of friction.

5.3 IC1000 Pad Stress Relaxation

5.3.1 Compressive Stress Relaxation

Pad samples were tested in a number of conditions to observe changes in compressive mechanical behavior during CMP. These conditions include: new and un-soaked, new and slurry soaked, new and distilled water soaked, and those used in planarization. Slurry or distilled water soaked pad samples were tested wet and dried. Samples used in planarization were taken from the performed planarization experiments that had polished the copper wafer at low pressure and high velocity. Six unused samples, two slurry soaked and wet samples, three distilled water soaked and wet samples, and two distilled water soaked and dried samples were tested. The remaining pad condition types tested had one sample each. The time averaged normalized stress versus time for the trials performed of the new and unused pad samples is shown in Fig. 5a. Also plotted on this figure are the time averaged normalized stress for the slurry soaked and wet pad sample trials. The error bars represent one standard deviation of the normalized stress through time for each respective pad condition type. The same relaxation data is plotted against a logarithmic time scale plus one, in Fig. 5b.

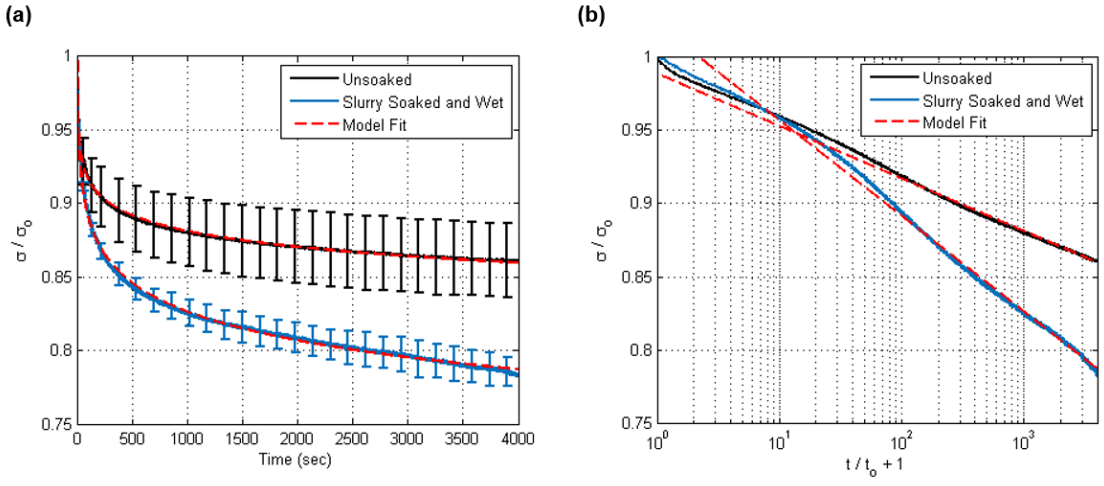

Fig. 5 Compression Stress Relaxation for New and Un-Soaked, Slurry Soaked and Wet Pad Samples at Initial Stress of 27.6 kPa **(a)** Normalized Stress versus Time with Standard Deviation Error Bars, **(b)** Normalized Stress versus Logarithmic Time plus One

This stress relaxation plot on a logarithmic time scale has a linear trend. A logarithmic stress relaxation model is proposed to describe the stress relaxation of the pad material over time, and is given in Equation 10,

$$\sigma = \sigma_o \left[k \cdot \log_{10} \left(\frac{t}{t_o} + 1 \right) + b \right] \tag{10}$$

k is the slope and *b* is the intercept of the line for normalized stress versus base-10 logarithm of unitless time plus one. The value of t_o is 1 second. The quantity of one is added to the normalized time within the logarithmic function since the logarithm of a quantity less than one is negative. A negative value of stress is meaningless for this model. Linear regressions are applied to the relaxation data of each pad sample type to acquire a best fit value for *k* and *b*. The fabricated compression testing system has a slight stress relaxation associated with it. This system relaxation was characterized and removed from the pad relaxation data to isolate the time-dependent behavior of the polishing pad alone. Using this stress relaxation model, a time constant is defined for comparisons between samples, as in Equation 11,

$$\tau_n = 10^{\left(-\frac{nb}{k}\right)} - t_o \tag{11}$$

τ_n is the time the sample takes to decrease a percentage *n* of its initial stress. As an example, 10% time constant values, $\tau_n = \tau_{0.1}$, from the fit stress relaxation models of all pad samples are given in Table 1.

Pad Sample	$\tau_{0.1}$ (seconds)	R^2
New, Un-Soaked	4842	0.995
New, Water Dried	220	0.998
New, Water Wet	122	0.999
New, Slurry Dried	622	0.985
New, Slurry Wet	65	0.996
Used, 50 Wafers	858	0.995
Used, 100 Wafers	379	0.993
Used, 250 Wafers	279	0.969

Table 1 10% Compressive Relaxation Time Constants for Polishing Pad Samples

From Table 1, the pad sample that had the largest relaxation time constant was un-soaked. The smallest relaxation time constants were those samples that were still wet when they were tested. These results show that the pad material relaxes stress more over time as water enters the IC1000 material structure. It has been reported in the literature that the pad material decreases in stiffness when it is soaked in water [17-20]. It is suggested by Castillo-Mejia, et al. that the decrease in stiffness is a result of the water breaking hydrogen bonds within the polyurethane. These relaxation results also show that the used samples had a decreasing trend in the time constant with increasing time polished. Overall, the stress relaxation data indicates that the polishing pad material relaxes more over time through use in CMP from soaking in slurry and increased polishing time. Less stress exerted by the pad on the wafer reduces its ability to form scratches, so these trends are important for the pad scratching process.

Additional stress relaxation experiments were performed at higher peak stresses to observe the effects of magnitude on pad relaxation behavior. At initial stresses of approximately 80 kPa and 170 kPa, the 10% time constants are computed to be 5.26 x 10^6 seconds and 1.19 x 10^{10} seconds, respectively. Both trials had coefficients of determination from their linear regression no less than 0.985. Comparing these values to the 10% time constant for 27.6 kPa equal to 4842 seconds, the pad material does not relax as much of its initial stress over time as the initial compressive stress increases.

5.3.2 Tensile Stress Relaxation

For the six new, un-soaked pad samples tested in tensile stress relaxation, the time dependent behavior can also be modeled well with the logarithmic relaxation model of Equation 10. An example of the tensile stress relaxation data of a sample held at 1% strain is shown in Fig. 6. Results of 10% time constants and the coefficients of determination for the tensile relaxation linear regressions are provided in Table 2.

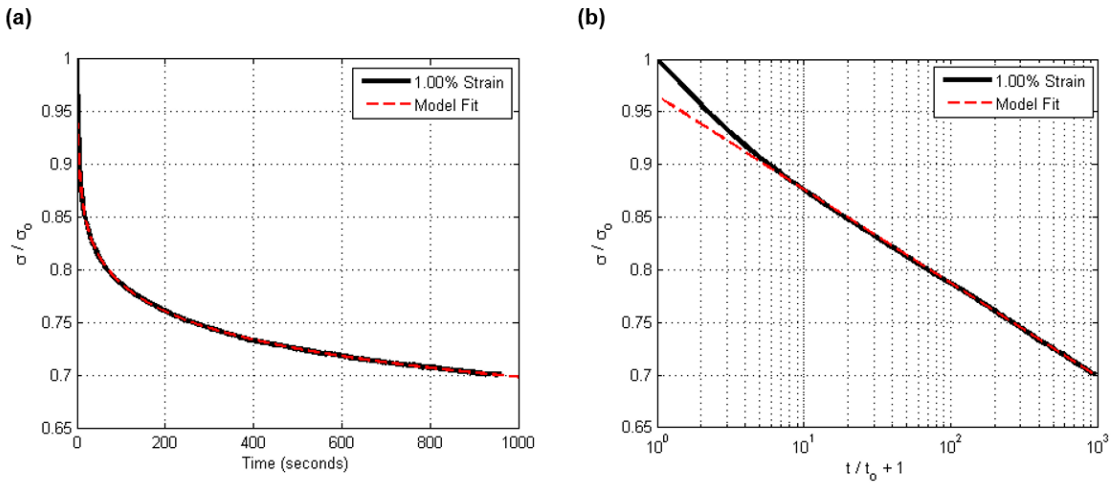

Fig. 6 Tensile Stress Relaxation for New and Un-Soaked Pad Sample at 1% Strain **(a)** Normalized Stress versus Time, **(b)** Normalized Stress versus Logarithmic Time plus One

Strain (%)	σ_o (kPa)	$\tau_{0.1}$ (seconds)	R^2
0.25	6.7 x 10^2	18.11	0.997
0.50	1.5 x 10^3	16.60	0.996
1.00	2.9 x 10^3	13.21	0.999
1.50	4.4 x 10^3	11.30	0.999
2.50	6.4 x 10^3	9.27	0.997
5.00	1.0 x 10^4	7.54	0.993

Table 2 10% Tensile Relaxation Time Constants for Un-Soaked Polishing Pad

For tensile stress relaxation experiments on IC1000 pad material, the 10% time constant decreases with increasing initial stress applied. This trend is opposite of the behavior found from compression relaxation experiments of the same pad material. Fig. 7 shows the differences in stress relaxation trends of the polishing pad with increasing initial stress. These results indicate that the IC1000 polishing pad material should be characterized in compression for proper constitutive

modeling of the pad for CMP. Additionally, the IC1000 polishing pad exhibited significant mechanical time dependent behavior with magnitudes of 10% time constant values between 10 seconds to 100 seconds. Thus, the viscoelastic strain energy term in the thermomechanical model of CMP from Equations 3 and 4 is non-zero. This mechanical behavior should be accounted for to properly model the mechanisms of CMP pad scratching.

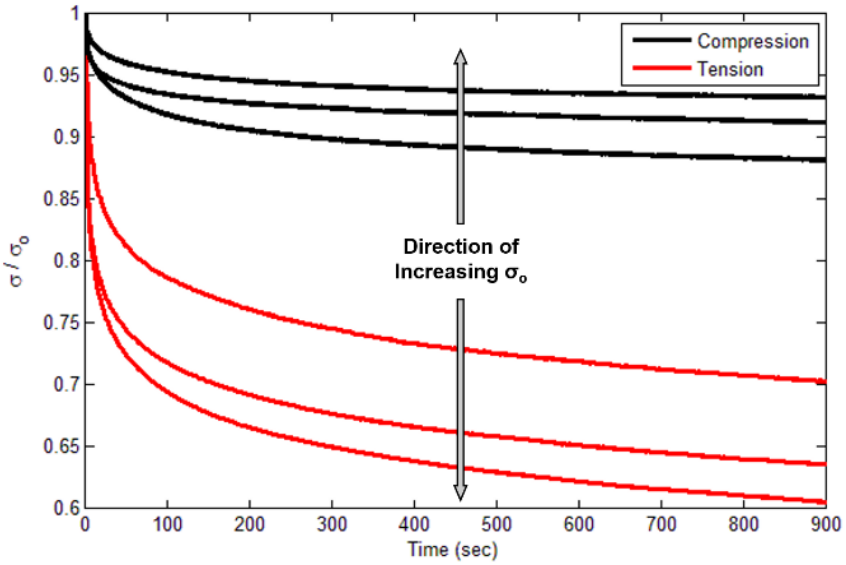

Fig. 7 Stress Relaxation of IC1000 in Compression and in Tension with Increasing Initial Stress

5.4 IC1000 Polishing Pad Compressibility

For each video frame of the compressed pad sample, the volume of pad material was estimated by the product of the thickness and the squared width. Dividing the current volume by the initial volume computes the approximate value of the Jacobian. An example of the Jacobian versus compressive strain for a single pad sample is presented in Fig. 8. Each data point represents the computed values of a single frame from the captured video.

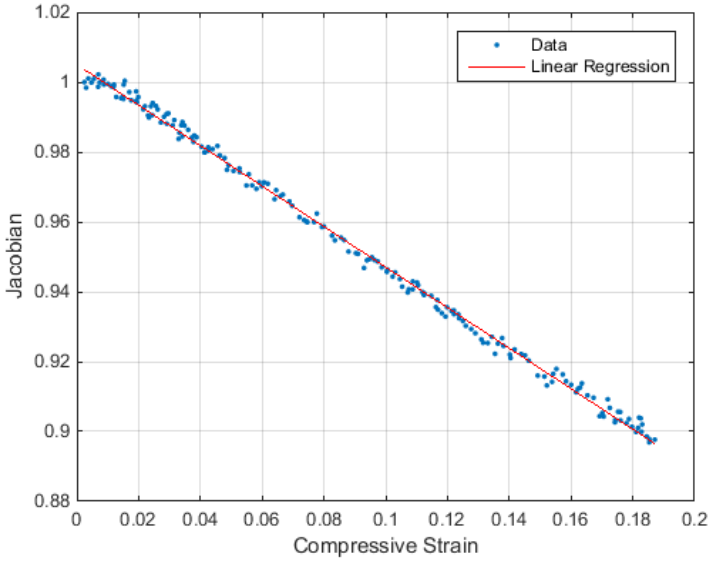

Fig. 8 Jacobian versus Axial Compressive Strain of IC1000 Sample with a Linear Regression

With the linear trend of the Jacobian with compressive strain, a linear regression is applied to this data for each of the eight trials performed. Coefficients of determination are no less than 0.992, representing good linear fit values for each respective trial. Slopes of the regression have a standard deviation that is approximately 20% of the average magnitude. This deviation may be explained as a result of the variations between shapes of pad samples. This estimate also assumes the friction that was acting on the compressed faces of the sample is negligible. Yet, the average fit model provides an approximation of the Jacobian. The regression coefficients are all trials averaged together for a representative Jacobian model, presented in Equation 12,

$$J = -0.590(\varepsilon_c) + 1.00 \tag{12}$$

A compressive strain, ε_c, of 5% gives an approximate Jacobian of 0.97. Equation 5 states that the true stress in the polishing pad material would be underestimated by 3% if the compressibility is not considered at 5% compressive strain. The compressibility of the pad material should be accounted for if the strains in the pad are large enough to significantly underestimate true stress.

From the same thickness and width computations, the Poisson's ratio and strain dilatation are determined. Based on the decrease in thickness for axial strain, and increase in width as transverse strain, the average Poisson's ratio for all pad samples was 0.25. Strain dilatation is equal to the unit volume change, or change in volume of the sample over the original sample volume. The unit volume change is the same as the Jacobian, except for the numerator in Equation 5 which is subtracted by the initial volume. Thus, the slope of dilatation with compressive strain is the same as in Equation 12, but the intercept is 0.

5.5 IC1000 Pad Differential Scanning Calorimetry (DSC)

For each DSC trial, the heat flow contributions from the difference in mass of the aluminum sample and reference pans are removed for each trial, assuming a constant specific heat of aluminum equal to 0.900 J/(g K) [21]. Specific heat values can be compared without contribution of the sample pan mass. The heat flow values were then normalized by the mass of the IC1000 pad sample tested. DSC mass normalized heat flow versus temperature for a tested new pad sample is presented in Fig. 9, where endotherms are negative. Each curve represents a separate portion of the DSC trial. The negative cooling curve represents the mass normalized heat flow multiplied by negative one, to allow for direct comparison between the first and second heating results. At the beginning of each heating or cooling curve, there was a sharp drop in the heat flow, which represents start-up transients of the DSC instrument. This behavior is a result of the larger heat capacity of the sample pan compared to the empty reference pan [22].

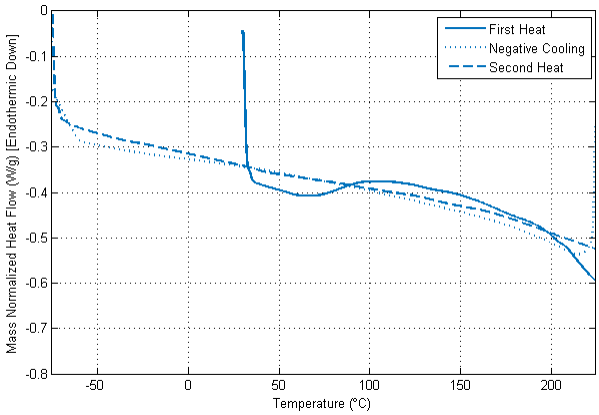

Fig. 9 Mass Normalized Heat Flow versus Temperature for a New IC1000 Pad Sample

Deviations in the heat flow of the first heating represent thermal reactions that occur within the pad material as it is heated. These reactions only occur in the first heating, thus they are irreversible reactions. The second heating and cooling curves have a negative linear trend with temperature. This downward trend corresponds to an increase of specific heat of the pad material, as more heat flow is required to increase the temperature at a constant rate. DSC trials were run for all four collected pad samples from eight different planarization experiments. Results from DSC of the pad samples from the planarization experiment with copper wafer, high pressure, and high velocity are shown in Fig. 10. Also plotted in this figure is the heat flow data from a new pad sample trial.

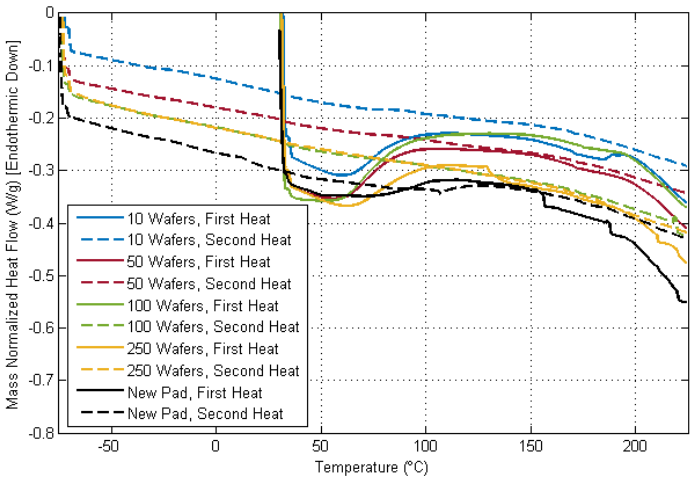

Fig. 10 Mass Normalized Heat Flow versus Temperature for Planarization Pad Samples (Copper, High Pressure, High Velocity)

Each trial shows similar trends in heat flow with slight deviations. The specific heat of pad samples have different values from sample to sample. To quantify any energy dissipated into the pad samples during the planarization experiments, the specific enthalpy of the irreversible reactions are computed from the area under the total first heat curve, using Equations 7 and 8. To remove influences of the shift in specific heat between trials, the second heat flow curves are shifted to all be equal at a single temperature. The temperature that is chosen does not significantly change the resulting trends in specific enthalpies. For an example in this report, 50°C was chosen as the shifting temperature. The first heat flow curves are then shifted by the same amount. The area under the curves are computed using trapezoidal numerical integration with MATLAB to compute specific enthalpies of reaction. Maximum error of the trapezoidal integration for specific enthalpy was estimated to be ± 1.8 J/g for a single trial. The average maximum error through all trials is ± 0.5 J/g. These values were estimated from errors of the trapezoidal rule using estimations of the second derivative of the data with respect to temperature from finite difference approximations [23].

The values of enthalpy of reaction and specific heat of second heating were statistically tested with the modified Thompson tau technique to identify outliers in the data [24]. Data points may be outliers due to artifacts of the experimental DSC trials which can provide results that are unrepresentative of the actual data set. Removal of outliers provides a better observation in actual trends in the data with the variables of interest. Values of enthalpy and specific heat of all trials that had polished the same number of wafers were compared between each other. The difference of each data point from the sample mean was compared to the product of the standard deviation of the data set and the corresponding Thompson tau value. If the difference is larger, the data point is statistically considered an outlier. Three outliers were found for specific enthalpy which include two of the new pad samples. The remaining outlier was found to be the enthalpy value from the copper wafer, high pressure, and high velocity planarization experiment sample at 100 wafers polished. No specific heat values for the second heating were found to be outliers. A figure that shows the specific enthalpies and specific heat values computed for the pad samples is provided in Fig. 11a and 11b.

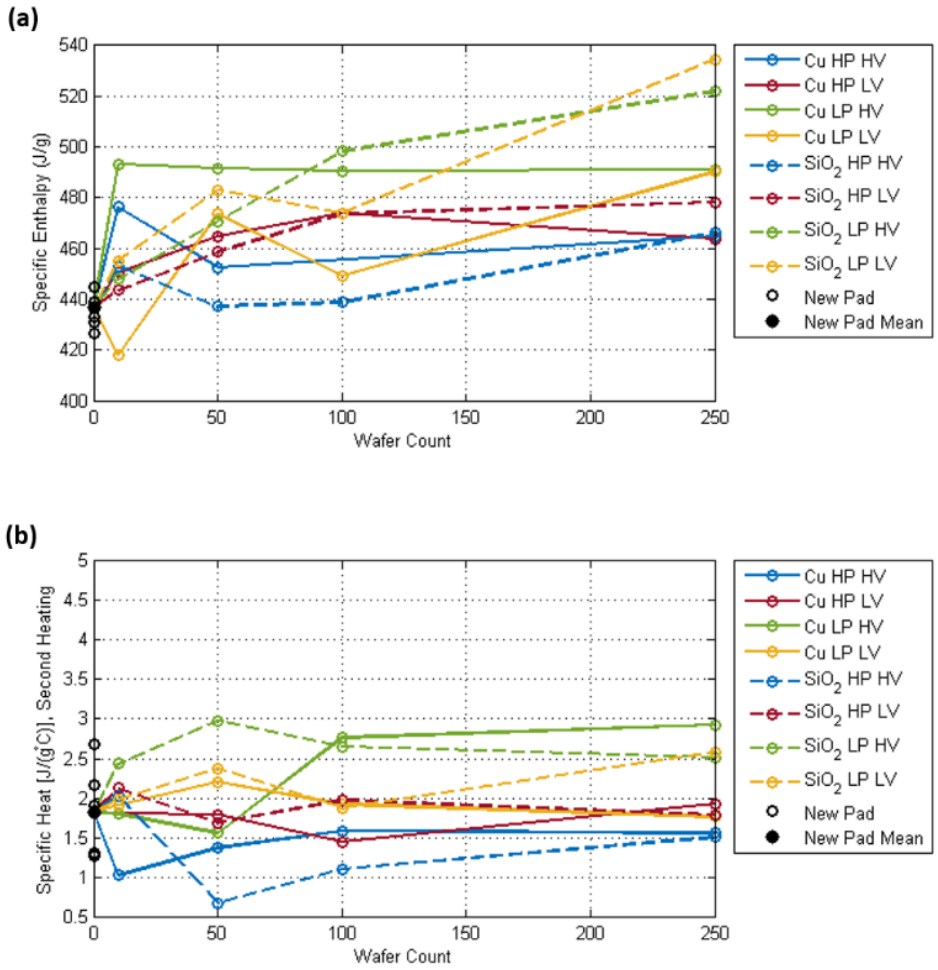

Fig. 11 IC1000 Pad DSC Analysis **(a)** Specific Enthalpy (Shifted Equal at 50°C), **(b)** Specific Heat of Second Heat at 50°C

Fig. 11a shows that the specific enthalpy has an increase with the number of wafers planarized from the new pad samples through 250 wafers. This increase in entropy suggests that energy was dissipated into the internal structure of the pad material surface through CMP. Thus, the chemical composition and potentially the mechanical behavior of the pad surface changes with as it planarized more wafers. Fig. 11b shows that there are no particular trends in specific heat with any other planarization experiment variable taken into account. The results for specific heat are very similar at any temperature taken as well as for second heat flow values. Reasons for the change in specific heats are currently unidentified; they may potentially be from physical changes of the polyurethane or artifacts of the experimental equipment.

5.6 Significance of Energy Dissipation for CMP Pad Scratching

Through experimental and theoretical methods, it has been found that the dissipation of energy during CMP affects the ability for the polishing pad to scratch the wafer surface. Several terms in the thermomechanical dissipation model represented in Equation 3 have been found to be nonzero and related to pad scratching criteria. DSC experiments performed on new and used polishing pad material show that the time rate of change of internal energy, $\dot{u}$, is positive in the pad material

due to a positive increase in the enthalpy of reaction with increasing polishing time. Increase in the internal energy of the pad material is a form of energy dissipation which alters the chemical composition of the pad material. Changes in chemical composition can potentially change mechanical properties which in turn can influence scratch production.

Rate of strain energy, $\boldsymbol{\sigma} : \boldsymbol{D}$, is another term in Equation 3 that has been found to be significant and related to scratch production. From the stress relaxation experiments in compression, both the elasto-plastic and viscoelastic strain energy terms in Equation 4 are shown to be important in the deformation of the polishing pad material at typical applied pressures during CMP. Additionally, a general decrease in surface roughness of the polishing pad with increasing polishing time demonstrates the significance of the plastic strain energy terms in Equation 4. From the theoretical stress field analysis, it was identified that the roughness of the polishing pad and changes in applied load between the pad and wafer contact have a large influence on the magnitudes of stresses induced within the wafer material. Thus, viscoelastic and plastic deformation directly influence the conditions of CMP wafer scratch production. The findings in this work demonstrate that the internal energy and strain energy dissipation terms in the thermomechanical model are significant and are related to pad scratch production in CMP.

6 Conclusions

A thermomechanical model was constructed to describe the pad scratching process in chemical-mechanical planarization. This provides a means to track the dissipation of energy input to the pad and wafer system. Identifying sources of energy dissipation provides a better physical understanding of CMP to account for processes that influence scratch production. Several dissipation processes were identified as significant through theoretical and experimental analysis. Viscoelastic mechanical behavior and compressibility of the polishing pad were determined to be significant in its constitutive behavior.

- A wafer stress field analysis with a pad asperity contact established that the ability for a polishing pad to scratch a wafer is reduced with a lower coefficient of friction between the pad and wafer, a smaller pad elastic modulus, and a smoother pad surface.
- Stress relaxation experiments performed on IC1000 polishing pad material displayed significant time-dependent mechanical behavior. Viscoelastic strain energy dissipation is essential in CMP modeling as a polishing pad that has been under stress for longer time will exert less stress on the wafer surface.
- Additionally, the polishing pad material relaxes its applied stress more over time through use in CMP from introduction of slurry into the material structure and increasing polishing time.
- Stress relaxation experiments in compression and in tension reveal that the pad material behaves mechanically different between both modes of deformation. Thus, the pad material should be mechanically characterized only in compression for proper polishing pad constitutive modeling.
- Plastic deformation of the polishing pad surface from surface smoothing during planarization has a potential correlation to the decrease in coefficient of friction between the pad and wafer. These results indicate that energy dissipation into plastic deformation of polishing pad material influences scratch production.

- DSC experiments on used pad material show an increase in energy dissipated into the surface of the polishing pad with more time polished. Energy dissipated into the internal structure of polishing pad material may have an important effect on its mechanical surface properties.

Significant sources of energy dissipation that influence pad scratching in CMP were identified. Additional analysis into the implications of these dissipation processes along with more explicit, quantitative modeling should be executed to obtain further physical understanding of the CMP process to prevent the formation of damage on IC wafers.

References

1. T. Eusner, N. Saka, and J.-H. Chun, J. Electrochem. Soc. **158**, H379 (2011)
2. S. Kim, N. Saka, J.-H. Chun, S.-H. Shin, CIRP Ann. Manuf. Technol. **62**, 307 (2013)
3. S. Kim, N. Saka, J.-H. Chun, ECS J. Solid State Sci. Technol. **3**, P169 (2014)
4. W. M. Lai, D. Rubin, E. Krempl, Introduction to Continuum Mechanics, 4th edn. (Elsevier, Burlington, 2010), p. 155
5. A. E. Green, P. M. Naghdi, Arch. Rotational Mech. Anal. **18**, 4 (1965)
6. G. A. Maugin, The Thermomechanics of Plasticity and Fracture, 1st edn. (Cambridge University Press, New York, 1992), p. 38
7. S. Balakumar, T. Haque, A. Senthil Kumar, M. Rahman, R. Kumar, J. Electrochem. Soc. **152**, G867 (2005)
8. A. Chandra, P. Karra, A. F. Bastawros, R. Biswas, P. J. Sherman, S. Armini, D.A. Lucca, CIRP Ann. Manuf. Technol. **57**, 559 (2008)
9. I. Li, K. Forsthoefel, K. A. Richardson, Y. Obeng, W. Easter, A. Maury, Mat. Res. Soc. Symp. **613**, E7.3.1 (2000)
10. H. Lu, Y. Obeng, K. A. Richardson, Mater. Charact. **49**, 177 (2003)
11. L. Charns, M. Sugiyama, A. Philipossian, Thin Solid Films **485**, 188 (2005)
12. S. Armini, C. M. Whelan, K. Maex, J. L. Hernandez, M. Moinpour, J. Electrochem. Soc. **154**, H667 (2007)
13. K. Dill, S. Bromberg, Molecular Driving Forces: Statistical Thermodynamics in Chemistry and Biology, 1st edn. (Garland Science, New York, 2003), p. 105
14. G. M. Hamilton, L. E. Goodman, J. Appl. Mech. **33**, 371 (1966)
15. G. M. Hamilton, Proc. Inst. Mech. Eng. C **197**, 1 (1983)
16. R. Budynas, J. Nisbett, Shigley's Mechanical Engineering Design, 9th edn. (McGraw-Hill, New York, 2011), p. 221
17. W. Li, D. Shin, M. Tomozawa, S. Murarka, Thin Solid Films **270**, 601 (1995)
18. M. Moinpour, A. Tregub, A. Oehler, K. Cadien, MRS Bull. **27**, 766 (2002)
19. D. Castillo-Mejia, S. Gold, V. Burrows, S. Beaudoin, J. Electrochem. Soc. **150**, G76 (2003)
20. B. Kim, M. Tucker, J. Kelchner, S. Beaudoin, IEEE Trans. Semicond. Manuf. **21**, 454 (2008)
21. J. Shackelford, W. Alexander, Materials Science and Engineering Handbook, 3rd edn. (CRC Press LLC, Boca Raton, 2001), p. 375
22. M. E. Brown, Handbook of Thermal Analysis and Calorimetry Volume 1: Principles and Practice, 1st edn. (Elsevier, Amsterdam, 1998), p. 279
23. E. Kreyszig, Advanced Engineering Mathematics, 10th edn. (John Wiley & Sons, Inc., New York, 2011), p. 827
24. M. S. Anbarasi, S. Ghaayathri, R. Kamaleswari, I. Abirami, Int. J. Comput. Sci. Inf. Technol. (IJCSIT) **2**, 1 (2011)